IEEE Access
Multidisciplinary | Rapid Review | Open Access Journal

Received March 25, 2020, accepted April 19, 2020, date of publication April 22, 2020, date of current version May 6, 2020.

Digital Object Identifier 10.1109/ACCESS.2020.2989521

Enhancing the Credibility of the Optical Performance Monitor With Adversarial Training

XIAOJIE FAN[1], YUWEI SU[2], TAO DONG[2], YIN JIE[2], YIYING ZHANG[1], FANG REN[1], JINGJING NIU[1], JINGYU ZHANG[1], AND JIANPING WANG[1]

[1]School of Computer and Communication Engineering, University of Science and Technology Beijing, Beijing 100083, China
[2]State Key Laboratory of Space-Ground Integrated Information Technology, Beijing Institute of Satellite Information Engineering, Beijing 100095, China

Corresponding author: Yuwei Su (suyuwei.love@163.com)

This work was supported in part by the Open Research Fund of the State Key Laboratory of Space-Ground Integrated Information Technology under Grant 2018-SGIIT-KFJJ-TX-10, in part by the National Natural Science Foundation of China (NSFC) under Grant 61671055, and in part by the Fundamental Research Funds for the Central University, China, under Grant FRF-TP-19-016A2.

ABSTRACT The existing optical performance monitoring (OPM) scheme based on deep neural network has no selection capability of the input data. They always accept and process all, which may result in serious monitoring errors and reduce the credibility of the monitoring system. Because the transmitted data in the future heterogeneous fiber-optic networks are diverse, and it's likely to exceed the scope of the monitoring system. We propose an unsupervised generative adversarial network (GAN) as the judgement module in the new OPM framework to select the legal data within the scope of the monitoring system. The generator consists of encoder-decoder-encoder (EDE) sub-network, jointly learns the image and latent feature distribution of the legal data. And the training data for the network in the new added judgement module is the same as the OPM analyzer network's, therefore, no extra data are collected, which is low-cost. In the simulation, four modulation formats under two bit-rates are taken into account to verify the model performance in the judgement module. When 60 Gbps 64QAM signal is selected as illegal data, the max value of the area under the curve (AUC) is 0.942. The judgement time for single image is about 12 ms. Moreover, the influence of the task weights and the latent feature shape on the judgement performance are investigated. The new added judgement module largely increases the credibility and safety of the existing OPM scheme.

INDEX TERMS Optical performance monitoring (OPM), generative adversarial network (GAN).

I. INTRODUCTION

With the high-speed development of various cutting-edge services, such as artificial intelligence (AI), fifth-generation (5G) and cloud computing, the data transmitted in optical fiber network is also increasing explosively. Moreover, in order to improve the quality-of-service (QoS) and meet the real-time needs of end-users, the optical network becomes more heterogeneous, dynamical and expecting a unified control and management of resources (e.g. bit-rate, modulation format., etc.) [1]. The elastic optical networks (EONs) together with software defined network (SDN) controllers can meet these demands. To ensure the reasonable control and management, it is crucial to provide correct and accurate monitoring parameters (e.g. modulation format, optical signal-to-noise ratio (OSNR), bit-rate, etc.) for the SDN controller using the technologies of OPM as well as bit-rate and modulation format identification (BR-MFI) [2]. The optical performance monitors deployed with the OPM and BR-MFI technologies are equipped on the various intermediate node of the optical network.

Recently, AI has attracted the attention of researchers, among which the deep learning (DL) technology has become a research hotspot in various areas such as natural language processing (NLP), computer vision (CV), automatic speech recognition (ASR), [3]–[5] etc. Compared with the traditional machine learning (ML) methods, DL has the significant advantages of self-learning and automatic feature extraction [6]. Naturally, with the purpose of improving the monitoring accuracy, more and more DL technologies are used in OPM [7] as well as BR-MFI [8], [9]. Moreover, some work even realize the BR-MFI and OPM simultaneously. In [10], [11], the convolutional neural network (ConvNet) was proposed for the BR-MFI and OPM by using the data of the eye-diagram

The associate editor coordinating the review of this manuscript and approving it for publication was Rentao Gu.

and constellation-diagram. In our previous works [12], the multi-task learning (MTL) based ConvNet was proposed for the OPM and BR-MFI by using the phase portrait images. Similarly, by using the asynchronous amplitude histogram (AAH), the MTL deep neural network (DNN) was proposed for the OPM and BR-MFI [13], [14]. In general, with the help of the advanced DL technologies, the result of the monitoring tasks (OPM and BR-MFI) are becoming more and more accurate.

However, there is a serious vulnerability in the existing OPM schemes when the optical performance monitor is deployed in the real monitoring scenario. Specifically, the analysis module of the existing OPM schemes directly use the supervised learning method to train the DL model as the data analyzer. A particular dataset is collected as the monitoring scope, then, based on this dataset, the DL model is trained to have an accurate monitoring result. In order for the trained DL model to work properly, an important premise is that the input data cannot exceed the monitoring scope, otherwise, the DL model will give a totally wrong result. Because the trained DL model can only give correct results within the monitoring scope. For example, if a QAM type signal is input into the analysis module which is only trained to identify the on-off keying (OOK) type signal, the analysis module would mistake the QAM signal for the OOK signal. For the optical performance monitor, the input data within the monitoring scope is defined as legal data, or else as illegal data. Unfortunately, the existing OPM schemes have no selection of the input data, which means that they accept and process all. Moreover, it is very easy for the optical performance monitor deployed in the heterogeneous optical network to receive the data exceeding the monitoring scope. Since the monitoring results are important for the SDN controller to manage and control the whole optical network, it is necessary for the optical performance monitor to have the ability of input data selection. The selection between the legal and illegal data can be solved as a supervised learning problem in theory, for example, we can put the illegal data into the training dataset, and train the DL model to recognize them. But there are endless illegal data types in the real monitoring scenario, which means that the DL model cannot filter the unknown illegal data while the training dataset is becoming bigger and bigger. In order to eliminate the vulnerability and improve the credibility of the optical performance monitor, more advanced technology and OPM framework are needed.

In this paper, we design a new OPM framework to improve the credibility in the practical monitoring scenario. Different from the old OPM framework which directly accepts and processes all the input data, a judgement module is added into the new OPM framework to filter the illegal data which exceeds the monitoring scope. The core of the judgement module is an unsupervised GAN which generator consists of EDE sub-network. The GAN model minimizes the distance between the images and latent features of the legal data during training. The large distance metric form the trained GAN model indicates illegal data. The asynchronous

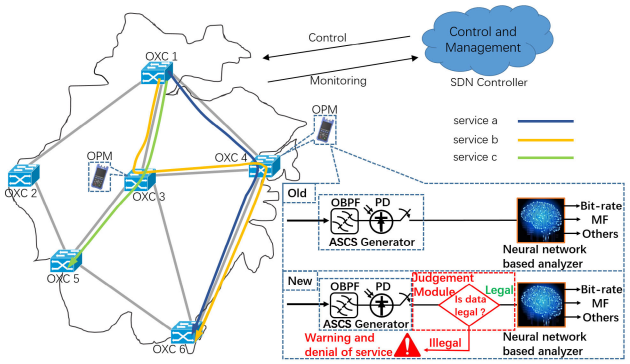

FIGURE 1. The proposed new OPM framework across the dynamic and heterogeneous optical network. OXC: optical cross-connect.

single channel sampling (ASCS) method is used to acquire the phase portrait images as the input data. Four common signals, 60/100 Gbps quadrature phase-shift keying (QPSK), 60/100 Gbps 4 quadrature amplitude modulation (QAM), 60/100 Gbps 16QAM, 60/100 Gbps 64QAM in the scenario of various impairments such as OSNR, chromatic dispersion (CD), and differential group delay (DGD) are comprehensively investigated to verify the performance of the judgement module. The good performance shows the effectiveness of the proposed OPM scheme.

II. METHODS

A. MORE CREDIBLE OPM FRAMEWORK

Firstly, we propose the new OPM framework based on the real monitoring scenario in the optical network, as shown in Fig. 1. Future heterogeneous optical network is designed to support various services (e.g. service a, b and c) with different parameters (e.g. OSNR, CD, DGD, modulation format, bit-rate, etc). For the better utilization of the resources in physical layer, it is necessary to use the optical performance monitor in the intermediate nodes to provide the monitoring information for the SDN controller. Based on the provided monitoring information, the SDN controller can formulate strategies to better control and manage resources. Thus, the optical performance monitors are required to provide as correct information as possible.

The old OPM framework simply consists of two modules: data generation and data analysis modules. The data generation module is used to continuously transform the network transmission signal into the data format (e.g. AAH, asynchronous delay-tap sampling (ADTS) images) suitable for the processing of the analysis module. Here, the phase portrait image is generated by the ASCS. The analysis module based on neural network will analyze the input data and then report the results. The neural network in the analysis module is pre-trained, which means that the monitoring scope is determined. Once the data which exceeds the monitoring scope is input into the analysis module, the totally wrong monitoring results are attained. However, in the development of the heterogeneous optical network, there will be more and

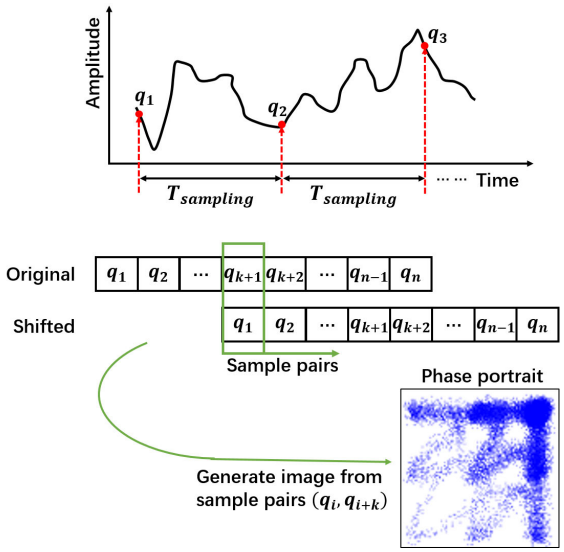

FIGURE 2. The generation principle of the ASCS phase portraits.

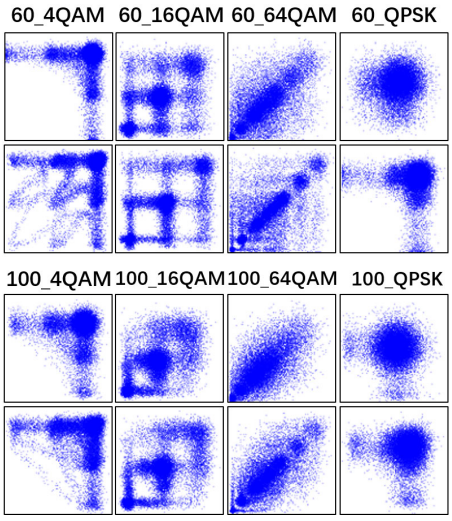

FIGURE 3. The phase portraits of all eight signals affected by various impairments. The first and the third rows correspond to OSNR = 12 dB without DGD and CD, the second and the forth rows correspond to OSNR = 24 dB, DGD = 4 ps and CD = 50 ps/nm.

more new services which can easily exceed the monitoring scope of the existing optical performance monitor. Without the ability to filter the illegal data, the monitoring information provided by optical performance monitor will lead to network chaos.

To solve this problem, we design a more credible OPM framework by adding a new judgement module on the old OPM framework. The new added judgement module located between the data generation module and the analysis module is used to filter the illegal data. Specifically, if the judgement module recognizes that the data generated by the data generation module is illegal, it will send out a warning and denial of service. Otherwise, the legal data will be sent to the analysis module to produce monitoring information. By adding the judgement module in the new OPM framework, the optical performance monitor becomes more credible, since it has the ability to filter illegal data so that the totally wrong monitoring information can be avoided. Moreover, since the judgement module and the analysis module are decoupled, the various monitoring algorithms studied by the predecessors can be applied without any modification.

B. ASYNCHRONOUS SINGLE CHANNEL SAMPLING

In the data generation module, we use the ASCS method to generate phase portrait images as the object of subsequent processing. The ASCS is a simple and low-cost method, since only the single-tap sampling without clock information is required [15], [16]. The principle of using the ASCS method to generate phase portraits is presented in Fig. 2. The optical signal transmitted in the network will be converted into electrical signal after being directly detected by the photodetector (PD). Then, the single-tap sampling with low rate $1/T_{sampling}$ is used to attain the original sample sequence marked as $q_1, q_2, \cdots q_N$. The shifted (shifted by k samples) version of the original sequence is attained to produce the sample pairs (q_i, q_{i+k}) together with the original sequence. The collected sample pairs are displayed as the phase portraits. Moreover, the different signals' phase portraits under diverse impairments are shown in Fig. 3. Obviously, the phase portraits can directly show the influence of various monitoring parameters, which are suitable for processing by the judgement and analysis modules.

C. ADVERSARIAL EDE CONVNET FOR DATA JUDGEMENT

After the data generation module, the phase portraits will be sent to the judgement module which is the focus in this paper. In the judgement module, the adversarial EDE ConvNet is proposed to filter the illegal data. The whole neural network model is designed on the framework of GAN invented by Goodfellow *et al.* [17]. As an unsupervised algorithm, GAN have been applied to various applications [18]–[23] because of its strong ability of learning data distribution. The basic idea of GAN is that the generator network G and the discriminator network D compete against each other in the training phase. Specifically, the generator network tries to learn the input data distribution and produce an image, then the discriminator network judges the authenticity (real or fake) of the generated image.

The overview of the adversarial EDE ConvNet is illustrated in Fig. 4. The generator is formed by an encoder-decoder-encoder sub-network. The generator learns the image and latent feature distribution by reconstructing the input image and extracted latent feature, respectively. Taking a $32 \times 32 \times 3$ color image I as the input of the generator, the first encoder sub-network G_{E1} downscales the input image to a feature Z of shape $1 \times 1 \times 100$. The feature Z which contains the most comprehensive information of the input image with the least size can be regarded as the input image's latent feature. Then, the decoder sub-network G_D reconstructs the

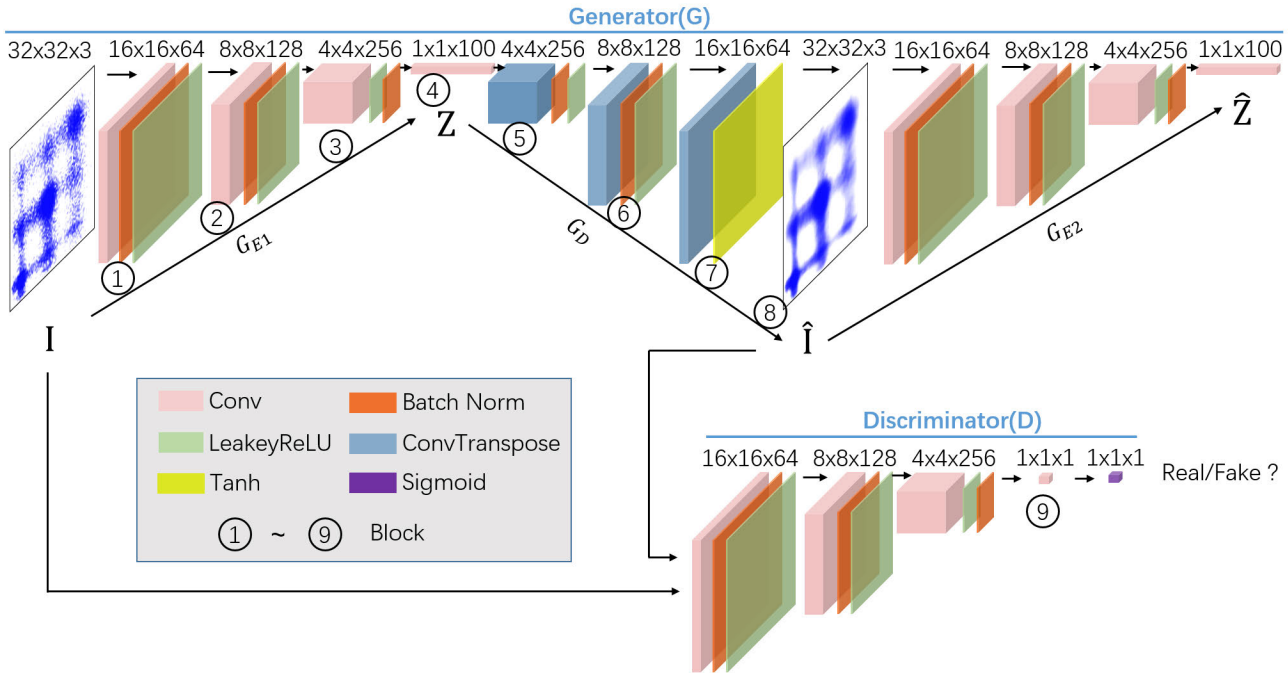

FIGURE 4. The architecture of the proposed adversarial EDE ConvNet in the judgement module.

TABLE 1. Details of the basic block.

Block number	1	2	3	4	5	6	7	8	9
Filter size	4	4	4	4	4	4	4	4	4
Stride	2	2	2	1	1	2	2	2	1
Padding	1	1	1	0	0	1	1	1	0
Channel	64	128	256	100	256	128	64	3	1

input image I as $\hat{I}$ by upscaling the feature Z. The G_{E1} consists of 4 layers, and each layer consists of convolutional operation, batch-norm and leaky ReLu() activation. Similarly, the G_D uses the convolutional transpose operation, ReLU() activation, batch-norm and the tanh() activation. Moreover, the second encoder sub-network G_{E2}, which has the same structure as G_{E1} but different weight parameters, is used to extract the latent feature $\hat{Z}$ from the reconstructed image $\hat{I}$. The feature $\hat{Z}$ has the same shape as feature Z. During training phase, the input image I and the reconstructed image $\hat{I}$ are identified by the discriminator network D as real and fake, respectively. With the help of the GAN framework, the EDE network can better learn the representation of the legal data. The details of the configuration (the filter size, stride, padding and number of channels) in the basic blocks are displayed in Table 1. To avoid repetition, the configuration of other blocks are omitted. Because other blocks are the reuse of the basic blocks, which means that they have the same structure and configuration.

In order to train the proposed model, a big training dataset denoted as $\{I_i\}_{i=1}^{M}$ is collected from the monitoring scope, where M is the number of the phase portraits and $I_i \in R^{32\times32\times3}$. Note that the training dataset only contains the legal data since the phase portraits are collected from the monitoring scope. Besides, a testing dataset of N phase portraits collected from both the inside and outside of the monitoring scope can be denoted as $\left\{\left(I_i', y_i\right)\right\}_{i=1}^{N}$, where the image label $y_i \in \{0, 1\}$ (0: illegal data, 1: legal data) and $I_i' \in R^{32\times32\times3}$. Based on the above two datasets, our model first learns the legal data distribution on the training dataset, then the trained model identifies whether the data in the testing dataset is legal or illegal. In the testing phase, a score $S\left(I_i'\right)$ indicating the probability of the input testing image being illegal will be calculated based on the L_2 distance of the latent features Z and $\hat{Z}$. The $S\left(I_i'\right)$ can be expressed as

$$S\left(I_i'\right) = \left\|G_{E1}\left(I_i'\right) - G\left(I_i'\right)\right\|_2 = \left\|Z - \hat{Z}\right\|_2 \tag{1}$$

The scores of the whole testing dataset are normalized to [0, 1]. The testing image I_i' is regarded as illegal when its score $S\left(I_i'\right)$ exceeds a certain threshold. During the training phase, the model is trained by the combined three loss functions. Each loss function is used to optimize the different part of the model. The first loss function is the adversarial loss. The most common way to train GAN is to update the generator G based on the output of the discriminator D, but this way is not stable. In order to alleviate the training instability, we use the feature matching [24] method to update G based on the $D's$ internal feature. Given an input image I_i from the distribution of training dataset, the feature matching method calculates the L_2 distance between the D's internal feature of the original image I_i and the reconstructed image $\hat{I}_i$, respectively. The

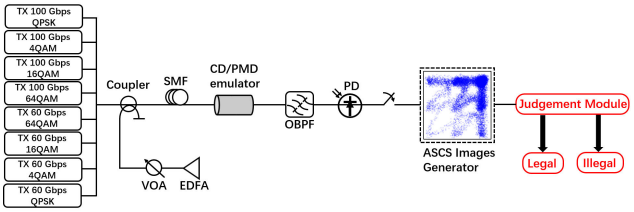

FIGURE 5. Simulation system for testing the performance of the judgement module.

adversarial loss can be expressed as

$$loss_{adv} = E_{x\sim px} \left\| f\left(I_i\right) - E_{x\sim px} f\left(\hat{I}_i\right) \right\|_2 \tag{2}$$

where $f(\cdot)$ is the output of the D's third layer. The second loss function is the reconstruction loss. It is used to optimize the G_{E1} and G_D by learning the content information about the input data. Since the L_1 distance produces less blurry image that the L_2 distance [19], we use the L_1 distance to define the reconstruction loss as

$$loss_{rec} = E_{x\sim px} \left\| I_i - \hat{I}_i \right\|_1 \tag{3}$$

The third loss function is the latent feature loss. The above two loss functions can enforce the G to learn the legal data distribution in image space, moreover, we add the latent feature loss to learn the distribution in latent feature space. The latent feature loss can be defined as

$$loss_{lat} = E_{x\sim px} \left\| Z - \hat{Z} \right\|_2 \tag{4}$$

Based on the three loss functions, the G learns the distribution of legal data both in image and feature space. When an illegal data which has different distribution with the legal data is inputted to the trained model, the distance between the latent features z and z' will increase beyond the threshold, since the model is trained only on legal data. Finally, the overall loss function can be expressed as

$$loss_{overall} = loss_{rec} + \lambda_1 loss_{lat} + \lambda_2 loss_{adv} \tag{5}$$

where λ_1 and λ_2 are the task weights to balance the influence of the latent feature loss and the adversarial loss, respectively. Two models with different important factors are trained for the comparison of performance. One model named as "Model 1" is trained when $\lambda_1 = 15$ and $\lambda_2 = 0$, which means that the "Model 1" is trained without the framework of GAN since $\lambda_2 = 0$. The other model named as "Model 2" is trained when $\lambda_1 = 15$ and $\lambda_2 = 5$. The specific information about the selection of the important factors is discussed in section B part III.

III. SYSTEM SETUP AND RESULTS

In order to collect data and build the neural network model, the simulation system is established on VPItransmissionMaker and Tensorflow library as shown in Fig. 5. Firstly, eight signals are generated in the transmitter by two bitrates (60/100 Gbps) and four common modulation formats (4QAM, 16QAM, QPSK and 64QAM). To simulate the impairments in single-mode fiber (SMF) transmission,

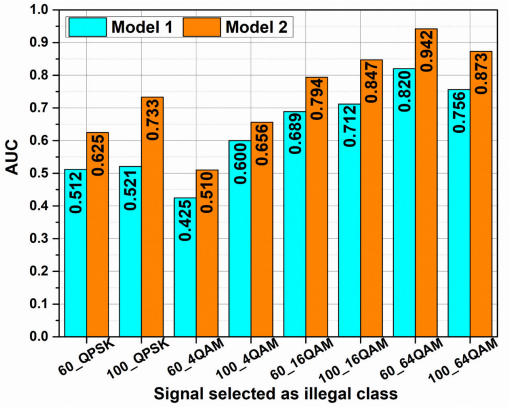

FIGURE 6. The AUC performance for the "Model 1" and "Model 2" when each signal type is selected as illegal class.

the CD/DGD emulator, the erbium-doped fiber amplifier (EDFA) as well as the variable optical attenuator (VOA) is used to add CD/DGD and OSNR, respectively. The values of OSNR, CD and DGD are adjusted in range 10-28 dB (the step is 2 dB), 0-450 ps/nm (the step is 50 ps/nm) and 0-10 ps (the step is 1 ps), respectively. The electrical signals are converted from the optical signals by PD. Then the ASCS method is used to generate phase portrait images (in ".png" format). Eventually, the phase portraits are sent to the adversarial EDE ConvNet in the judgement module to identify whether it is legal or illegal.

For each combination of the modulation format and bitrate, we collect 1100 ($10 \times 10 \times 11$) phase portraits. Therefore, for the eights signals, a large dataset comprises of 8800 (1100×8) phase portraits is collected. To simulate different monitoring scope, we treat each type of signal as the illegal data, while the rest seven signals are regarded as the legal data in the monitoring scope. Totally, eight sets of dataset are prepared, each of which regarded the individual signal as the illegal data. For each set of dataset, the legal data (7700 images) are randomly split into the training dataset and the testing dataset according to the proportion of 6/7 (6600 images) and 1/7 (1100 images), respectively. Finally, the illegal data (1100 images) would be combined into the testing dataset which split from legal data as the final testing dataset (2200 images). Generally, there are eight sets of data, and each set of data has the training dataset (6600 legal images) and the testing dataset (2200 images of mixed legal and illegal data). Note that in the actual optical performance monitor, the judgement module and the analysis module are trained on the identical training data, therefore, no extra data are needed for the new added judgement module, which is low-cost. The proposed adversarial EDE ConvNet is optimized by the Kinga and Adam [25] on the overall loss function with the learning rate $lr = 2e^{-3}$ and momentums $\beta_1 = 0.46$, $\beta_2 = 0.986$.

A. THE PERFORMANCE OF DATA JUDGEMENT

Firstly, for each signal selected as the illegal data, the AUC values of the "Model 1" and "Model 2" are presented in

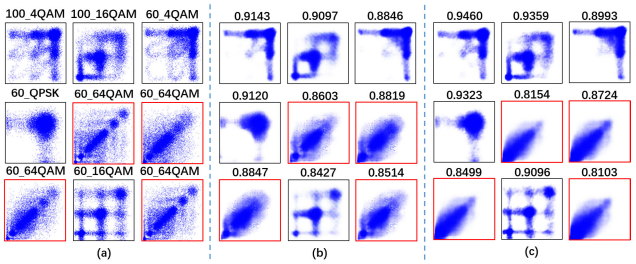

FIGURE 7. (a) The original input images. (b) The corresponding reconstructed images by the "Model 1". (c) The corresponding reconstructed images by the "Model 2". The images with red border indicate the illegal data. The correlation values between the reconstructed and the input images are displayed at the top of each reconstructed image.

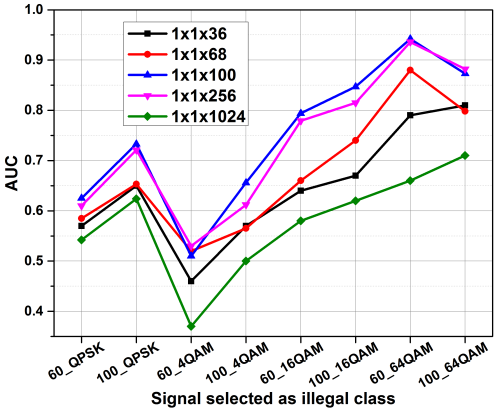

FIGURE 8. The AUC performance in response to the latent feature shape when each signal type is selected as the illegal class.

Fig. 6. The definition of AUC is that the area under the Receiver Operating Characteristic (ROC) curve, which is often used to evaluate the binary classifier's performance. The classifier corresponding to the bigger AUC has a better performance. Obviously, the "Model 2" achieves higher AUC than the "Model 1" for all illegal classes. The highest AUC 0.820 and 0.942 are achieved by the "Model 1" and "Model 2", respectively, when the 60 Gbps 64QAM is selected as the illegal class. The lowest AUC 0.425 and 0.510 are achieved by the "Model 1" and "Model 2", respectively, when the 60 Gbps 4QAM is selected as the illegal class. The results show that with the help of the GAN framework, the "Model 2" ($\lambda_2 = 5$) can better fit the data distribution of the monitoring scope.

Moreover, select the highest AUC models (the "Model 1" and "Model 2" when 60 Gbps 64QAM is selected as illegal class) as the research objects, some examples of the input images, and the corresponding reconstructed images (reconstructed by the "Model 1" and "Model 2", respectively) are illustrated in Fig. 7, in which the images with red border are the illegal data (60 Gbps 64QAM). The Fig. 7(a) shows the input images. The Fig. 7(b) and Fig. 7(c) shows the corresponding reconstructed images of the Fig. 7(a) by the "Model 1" and "Model 2", respectively. The correlation between the reconstructed and the input images are displayed at the top of each reconstructed image in Fig. 7(b) and 7(c). Since the reconstructed legal images have the better image content and the bigger correlation value than the reconstructed illegal images, we can conclude that both the two models can effectively reconstruct the legal images, but fail to reconstruct the illegal images. It is because that the trained model have learned the legal data distribution, so it is easy to reconstruct legal image rather than the illegal image. The difference of the reconstruction performance between the legal and illegal images is an intuitive reflection of the distribution difference between the legal and illegal data. For the legal images, the reconstruction performance of the "Model 2" is better than the reconstruction performance of the "Model 1", while, for the illegal images, the reconstruction performance of the "Model 2" is worse than the reconstruction performance of the "Model 1". This means that the "Model 2" which trained on the GAN framework is more powerful in identifying the illegal data.

B. LATENT VECTOR LENGTH AND TASK WEIGHT

The latent features Z and $\hat{Z}$ are used to represent the data distribution, the shape of the latent feature would directly affect the representation ability of the data distribution, then affect the model performance of identifying illegal data. Besides, the task weights also affects the model performance. Therefore, it is necessary to study how these hyper-parameters affect the model performance. Here, we take the "Model 2" as the research object and change the shape of its latent feature. The AUC values for each latent feature shape under different monitoring scope are illustrated in Fig. 8. It is clear that when the shape of the latent feature is $1 \times 1 \times 100$, the model achieves best AUC for almost all monitoring scope. To be more concrete, when the length of the third dimension is less than 100, the larger the third dimension is, the better the model performance is. Nevertheless, once the length of the third dimension exceeds 100, the model performance begins to decline. It is because that small shape cannot contain all the useful features, while large shape contains too much redundant features.

Next, the influence of the task weights on the model performance is studied when the shape of the latent feature is fixed at $1 \times 1 \times 100$ and 60 Gbps 64QAM is selected as the illegal data, as shown in Fig. 9. The task weights are adjusted in the range of [0, 30] with the step of 5. Obviously, when the task weight λ_2 is at the range of [0, 15] and the task weight λ_1 is at the range of [0, 10], the model performance is poor (AUC is about less than 0.5084). When the λ_1 is at the range of [10, 20] and the λ_2 is at the range of [0, 10], the model achieves good performance. The optimal model performance (the AUC value is 0.9420) is achieved when the λ_1 equals 15 and the λ_2 equals 5, which is exactly the task weights configuration of the "Model 2".

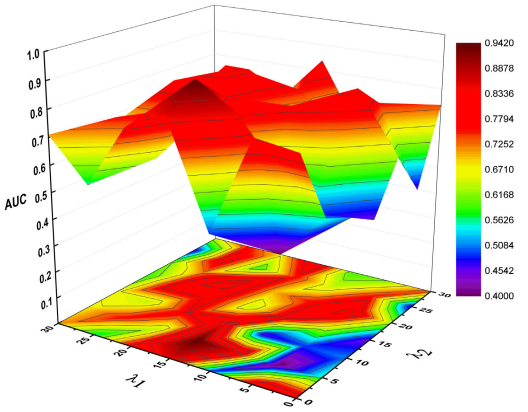

FIGURE 9. The AUC performance in response to the task weights of λ_1 and λ_2.

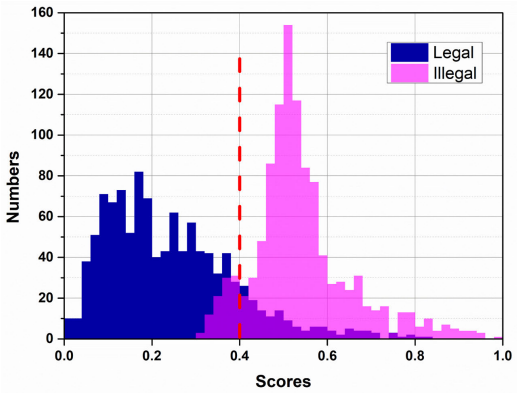

FIGURE 10. Histogram of the judgement scores for the images in the testing dataset.

Generally, in order to make the model have good performance, it is very important to select the appropriate shape of the latent features and the task weights. In the case of this paper, it is suitable to set the latent feature shape, the λ_1 and the λ_2 to $1 \times 1 \times 100$, 15 and 5, respectively.

C. DISTRIBUTION OF THE JUDGEMENT SCORES AND FEATURES

The "Model 2" trained when the 60 Gbps 64QAM signal is selected as the illegal data is used to evaluate the corresponding testing dataset. The histogram of the judgement score $S\left(I_i'\right)$ during the test phase is illustrated in Fig. 10. It is clear that a separation score around 0.4 can effectively separate the testing data into the legal data and illegal data. Although the legal data and the illegal data have the overlapping parts, the proportion of the overlapping parts is very small, which has a limited impact on the overall performance. Moreover, the t-SNE [26] visualization of the extracted features from the third layer ($f(\cdot)$) of the discriminator network D is illustrated in Fig. 11. The shape of the feature produced from the third layer of the D is $4 \times 4 \times 256$. The t-SNE is a non-liner dimensionality reduction algorithm, which is common for

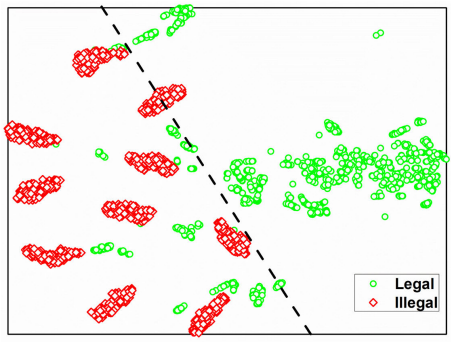

FIGURE 11. The t-SNE visualization of the extracted features from the third layer of the discriminator network.

visualization. It is obvious that the legal data and illegal data can be roughly separated into two parts, which means that the discriminator network D has the ability to identify whether the data is legal or not. The above results directly prove the validity of the proposed model. Based on the Intel Core i7 CPU, the average time for the model to process each image in the testing dataset is around 12 ms, which can be shorter by using the Graphics Processing Unit (GPU) devices. Compared with the old OPM framework, although the new added judgement module increases the processing time of the data (within an acceptable range), it greatly enhances the credibility of the optical performance monitor, which is of great significance to the development of the optical network.

IV. CONCLUSION

In conclusion, an adversarial EDE network as the new added judgement module in the new OPM framework is proposed. The new OPM framework as well as the adversarial EDE network can filter the data which exceed the monitoring scope of the optical performance monitor, so as to avoid the totally wrong monitoring results. By the comparison of the EDE network (without GAN framework), the proposed adversarial EDE network achieves better performance. When 60 Gbps 64QAM signal is selected as illegal data, the max value of the AUC is 0.942. A short time around 12 ms is taken for our model to process a single input image, which is very efficient. The judgement module and the analysis module are trained on the identical training data, therefore, no extra data are needed for the new added judgement module, which is convenient and low-cost. Moreover, the effects of the latent feature shape and the task weights on the model performance were studied in detail. The proposed method is of great significance to enhance the credibility of the optical performance monitor and assure the efficient operation of the optical network.

REFERENCES

[1] Q. Zhuge and W. Hu, "Application of machine learning in elastic optical networks," in *Proc. Eur. Conf. Opt. Commun. (ECOC)*, Rome, Italy, Sep. 2018, pp. 1–3.
[2] Z. Dong, F. N. Khan, Q. Sui, K. Zhong, C. Lu, and A. P. T. Lau, "Optical performance monitoring: A review of current and future technologies," *J. Lightw. Technol.*, vol. 34, no. 2, pp. 525–543, Jan. 15, 2016.

[3] Y. Zhang, M. Pezeshki, P. Brakel, S. Zhang, C. Laurent, Y. Bengio, and A. Courville, "Towards End-to-End speech recognition with deep convolutional neural networks," in *Proc. Interspeech*, Sep. 2016, pp. 1–5.
[4] A. Krizhevsky, I. Sutskever, and G. E. Hinton, "ImageNet classification with deep convolutional neural networks," in *Proc. Int. Conf. Neural Inf. Process. Syst.*, 2012, pp. 1097–1105.
[5] X. Zhang, J. Zhao, and Y. Lecun, "Character-level convolutional networks for text classification," in *Proc. Conf. Workshop Neural Inf. Process. Syst.*, 2015, pp. 649–657.
[6] X. Fan, Y. Xie, F. Ren, Y. Zhang, X. Huang, W. Chen, T. Zhangsun, and J. Wang, "Joint optical performance monitoring and modulation Format/Bit-rate identification by CNN-based multi-task learning," *IEEE Photon. J.*, vol. 10, no. 5, pp. 1–12, Oct. 2018.
[7] T. Tanimura, T. Hoshida, T. Kato, S. Watanabe, and H. Morikawa, "Convolutional neural network-based optical performance monitoring for optical transport networks," *J. Opt. Commun. Netw.*, vol. 11, no. 1, pp. A52–A59, Jan. 2019.
[8] J. Zhang, W. Chen, M. Gao, Y. Ma, Y. Zhao, W. Chen, and G. Shen, "Intelligent adaptive coherent optical receiver based on convolutional neural network and clustering algorithm," *Opt. Express*, vol. 26, no. 14, pp. 18684–18698, Jul. 2018.
[9] W. Zhang, D. Zhu, Z. He, N. Zhang, X. Zhang, H. Zhang, and Y. Li, "Identifying modulation formats through 2D Stokes planes with deep neural networks," *Opt. Express*, vol. 26, no. 18, pp. 23507–23517, Sep. 2018.
[10] D. Wang, M. Zhang, J. Li, Z. Li, J. Li, C. Song, and X. Chen, "Intelligent constellation diagram analyzer using convolutional neural network-based deep learning," *Opt. Express*, vol. 25, no. 15, pp. 17150–17166, Jul. 2017.
[11] D. Wang, M. Zhang, Z. Li, J. Li, M. Fu, Y. Cui, and X. Chen, "Modulation format recognition and OSNR estimation using CNN-based deep learning," *IEEE Photon. Technol. Lett.*, vol. 29, no. 19, pp. 1667–1670, Oct. 1, 2017.
[12] X. Fan, L. Wang, F. Ren, Y. Xie, X. Lu, Y. Zhang, T. Zhangsun, W. Chen, and J. Wang, "Feature fusion-based multi-task ConvNet for simultaneous optical performance monitoring and bit-Rate/Modulation format identification," *IEEE Access*, vol. 7, pp. 126709–126719, 2019.
[13] Z. Wan, Z. Yu, L. Shu, Y. Zhao, H. Zhang, and K. Xu, "Intelligent optical performance monitor using multi-task learning based artificial neural network," *Opt. Express*, vol. 27, no. 8, pp. 11281–11291, Apr. 2019.
[14] Y. Cheng, S. Fu, M. Tang, and D. Liu, "Multi-task deep neural network (MT-DNN) enabled optical performance monitoring from directly detected PDM-QAM signals," *Opt. Express*, vol. 27, no. 13, pp. 19062–19074, Jun. 2019.
[15] Y. Yu and C. Yu, "OSNR monitoring by using single sampling channel generated 2-D phase portrait," in *Proc. Opt. Fiber Commun. Conf.*, Mar. 2014, pp. 1–3.
[16] Y. Yu and C. Yu, "Optical signal to noise ratio monitoring using variable phase difference phase portrait with software synchronization," *Opt. Express*, vol. 23, no. 9, pp. 11284–11289, May 2015.
[17] I. P.-A. J. Goodfellow, M. Mirza, B. Xu, D. Warde-Farley, S. Ozair, A. Courville, and Y. Bengio, "Generative adversarial nets," in *Proc. Adv. Neural Inf. Process. Syst.*, 2014, pp. 2672–2680.
[18] Y. Choi, M. Choi, M. Kim, J.-W. Ha, S. Kim, and J. Choo, "StarGAN: Unified generative adversarial networks for multi-domain image-to-image translation," in *Proc. IEEE/CVF Conf. Comput. Vis. Pattern Recognit.*, Jun. 2018, pp. 8789–8797.
[19] P. Isola, J.-Y. Zhu, T. Zhou, and A. A. Efros, "Image-to-image translation with conditional adversarial networks," in *Proc. IEEE Conf. Comput. Vis. Pattern Recognit. (CVPR)*, Jul. 2017, pp. 5967–5976.
[20] B. K. Beaulieu-Jones, Z. S. Wu, C. Williams, R. Lee, S. P. Bhavnani, J. B. Byrd, and C. S. Greene, "Privacy-preserving generative deep neural networks support clinical data sharing," *Circulat., Cardiovascular Qual. Outcomes*, vol. 12, no. 7, Jul. 2019, Art. no. e005122.
[21] Y. Saito, S. Takamichi, and H. Saruwatari, "Statistical parametric speech synthesis incorporating generative adversarial networks," *IEEE/ACM Trans. Audio, Speech, Lang. Process.*, vol. 26, no. 1, pp. 84–96, Jan. 2018.
[22] Y. Zhao, S. Takaki, H.-T. Luong, J. Yamagishi, D. Saito, and N. Minematsu, "Wasserstein GAN and waveform loss-based acoustic model training for multi-speaker text-to-speech synthesis systems using a WaveNet vocoder," *IEEE Access*, vol. 6, pp. 60478–60488, 2018.
[23] A. Radford, L. Metz, and S. Chintala, "Unsupervised representation learning with deep convolutional generative adversarial networks," *Comput. Sci.*, vol. 2, no. 3, pp. 34–38, Nov. 2015.
[24] T. Salimans, I. Goodfellow, W. Zaremba, V. Cheung, A. Radford, and X. Chen, "Improved techniques for training gans," in *Proc. Adv. Neural Inf. Process. Syst.*, 2016, pp. 2234–2242.
[25] D. Kinga and J. B. Adam, "Adam: A method for stochastic optimization," in *Proc. Int. Conf. Learn. Representations*, vol. 5, 2015, pp. 1–15.
[26] D. M. L. Van and G. Hinton, "Visualizing data using t-SNE," *J. Mach. Learn. Res.*, vol. 1, pp. 1–48, Nov. 2008.

XIAOJIE FAN received the bachelor's degree in communication engineering from the University of Science and Technology Beijing, Beijing, China, in 2017, where he is currently pursuing the Ph.D. degree with the School of Computer and Communication Engineering. His research interests include optical communication and deep learning.

YUWEI SU received the B.E. degree from the University of Electronic Science and Technology of China, Chengdu, China, in 2012, and the M.S. and Ph.D. degrees from Waseda University, Tokyo, Japan, in 2014 and 2018, respectively. He is currently an Engineer with the State Key Laboratory of Space-Ground Integrated Information Technology, Beijing Institute of Satellite Information Engineering. His research interests include free space optical communications, space optical networks, adaptive optics, and atmospheric turbulence compensation technologies.

TAO DONG received the B.S. and Ph.D. degrees in electronics science and technology from the Beijing Institute of Technology, in 1999 and 2004, respectively. He is currently a Professor with the State Key Laboratory of Space-Ground Integrated Information Technology, Beijing Institute of Satellite Information Engineering. His research interests include antenna, optical phased array, free space optical communication, and space optical networks.

YIN JIE received the B.E. and Ph.D. degrees from the Beijing University of Posts and Telecommunications, in 2005 and 2010, respectively. He is currently a Senior Engineer with the State Key Laboratory of Space-Ground Integrated Information Technology, Beijing Institute of Satellite Information Engineering. His research interests include free space optical communications, space optical networks, and microwave photonics.

YIYING ZHANG received the bachelor's degree in communication engineering from the University of Science and Technology Beijing, Beijing, China, in 2015, where she is currently pursuing the Ph.D. degree with the School of Computer and Communication Engineering. Her research interest includes optical communications.

FANG REN received the bachelor's and master's degrees in electronic science and technology from Tianjin University, Tianjin, China, in 2008 and 2010, respectively, and the Ph.D. degree in information electronics from Hokkaido University, Sapporo, Japan, in 2014. Her research interests include optical communication systems, optical devices, and deep learning.

JINGJING NIU received the bachelor's degree in communication engineering from the University of Science and Technology Beijing, Beijing, China, in 2019, where she is currently pursuing the master's degree with the School of Computer and Communication Engineering. Her research interest includes optical communications.

JINGYU ZHANG received the bachelor's degree in communication engineering from the University of Science and Technology Beijing, Beijing, China, in 2019, where she is currently pursuing the master's degree with the School of Computer and Communication Engineering. Her research interests include deep learning and robotics.

JIANPING WANG received the bachelor's, master's, and Ph.D. degrees from the School of Precision Instrument and Optoelectronic Engineering, Tianjin University, Tianjin, China, in 1995, 1997, and 2000, respectively. Her research interests include optical communications, microwave photonics, and deep learning.